Supporting Information for:

Molecular Heaters: A green route to boosting crop yields?

Jack. M. Woolley,[‡,a] Natercia d. N. Rodrigues,[‡,a] Josene M. Toldo,[‡,b]* Benjamin Rioux,[‡,c] Chris Groves,[‡,d] Xandra Schrama,[‡,e] Jimmy Alarcan,[‡,f] Temitope T. Abiola,[a] Matthieu M. Mention,[c] Mariana T. do Casal,[b] S.E. Greenough,[a] Marise Borja,[g] Wybren J. Buma,[h,i]* Michael N.R. Ashfold,[j]* Albert Braeuning,[f]* Teun Munnik,[e]* Keara A. Franklin,[d]* Florent Allais,[c]* Mario Barbatti,[b,k] and Vasilios G. Stavros[a,l]*

a Department of Chemistry, University of Warwick, Coventry, CV4 7AL, United Kingdom.

b Aix Marseille University, CNRS, ICR, Marseille, France.

c URD, Agro-Biotechnologies Industrielles (ABI), CEBB AgroParisTech, 51110 Pomacle, France.

d School of Biological Sciences, University of Bristol, Bristol, BS8 1TQ, United Kingdom.

e Section Plant Cell Biology, University of Amsterdam, Amsterdam, The Netherlands.

f Department of Food Safety, German Federal Institute for Risk Assessment, Max-Dohrn-Str. 8-10, 10589, Berlin, Germany.

g GAB Consulting Spain S.L.U., Calle Gregorio Mayans 3, pta. 10 46005 Valencia, Spain.

h Van 't Hoff Institute for Molecular Sciences, University of Amsterdam, Amsterdam, The Netherlands.

i Institute for Molecules and Materials, FELIX Laboratory, Radboud University, 6525 ED Nijmegen, The Netherlands.

j School of Chemistry, University of Bristol, Cantocks Close, Bristol, BS8 1TS, United Kingdom.

k Institut Universitaire de France, 75231 Paris, France.

l School of Chemistry, University of Birmingham, Birmingham, B15 2TT, United Kingdom

1. Additional Spectroscopic Data

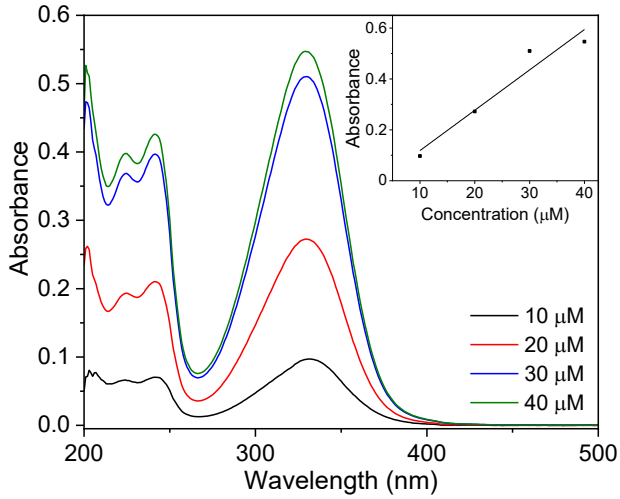

Figure S1. UV/Vis absorption spectra of SDA solvated in ethanol at various concentrations. The inset shows a linear fit of the peak absorbance (at 330 nm) *vs* sample concentration, the gradient of which yields the molar extinction coefficient ε =15000 ± 2000 M^{-1} cm^{-1}.

2. Transient Absorption Fitting and Residuals

The Transient Electronic Absorption Spectroscopy (TEAS) data collected in this work is inherently chirped as a consequence of group velocity dispersion (i.e. each probe wavelength has a different time zero).[1] The TAS data displayed in Figure 2 of the main paper have been manually chirp corrected using the program KOALA to aid visualization.[2] To extract dynamical information, the collected TAS data were globally fitted in R using the Glotaran interface.[3,4] This program models the chirp as a third order polynomial ($n = 3$) of the following function:

$$\mu(\lambda)=\mu_0+\sum_{i=1}^{n}\mu_i\left(\frac{\lambda-\lambda_c}{100}\right)^i \quad (1)$$

where $\mu(\lambda)$ is the time zero for a given wavelength and μ_0 is the time zero at the user defined central wavelength λ_c. Glotaran then models the data matrix ψ for each probe wavelength (λ_{pr}) and time delay (Δt) as a superposition of n components. All TAS data in this paper are described by three components ($n = 3$) in a sequential model $\left(A \overset{\tau_1}{\rightarrow} B \overset{\tau_2}{\rightarrow} C \overset{\tau_3}{\rightarrow} D\right)$ in the following manner:

$$\psi(\lambda, t) = \sum_l^{n_{comp}} c_l^{EADS}(t,\theta)EADS_l(\lambda) \quad (2)$$

Here, c_l^{EADS} is the exponentially decaying concentration of component l convoluted with a Gaussian instrument response function and $EADS_l(\lambda)$ is the evolutionary associated difference spectrum (EADS) associated with compartment l. For each set of initial parameters θ, the fit is iterated until a convergence criterion is reached. The fit is then reported as a combination of lifetimes τ_l and $EADS_l$. The quality of the fit is judged by the residuals (data minus fit). Residuals for the fitting of all the TAS data displayed in the paper are displayed in Figure S2.

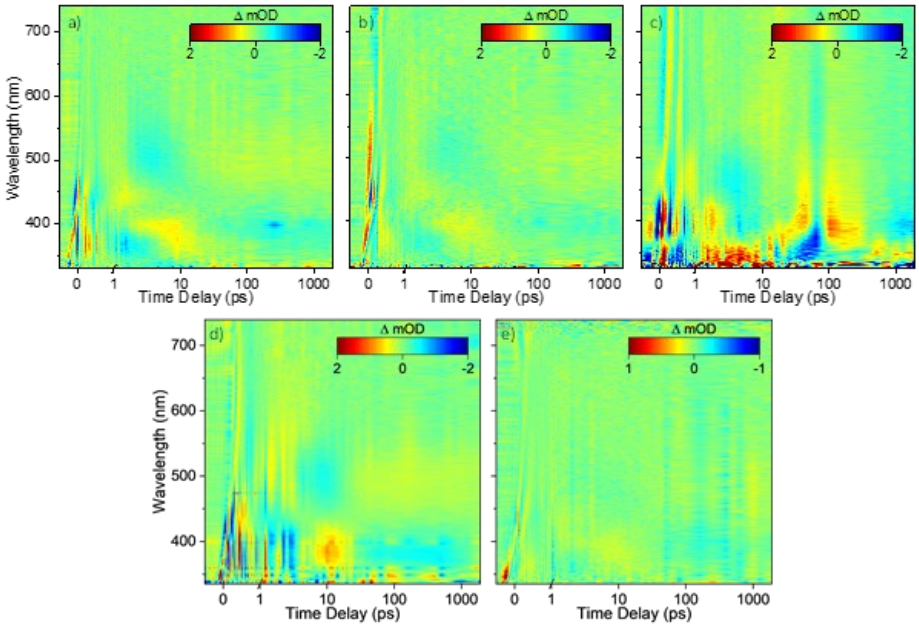

Figure S2. False colour heat maps of the fitting residuals of SDA TAS data recorded using: a) 10 mM aqueous solution, pH 5.6, 100 µm sample spacing; b) 10 mM aqueous solution, pH 5.6, 6 µm sample spacing against the cuticle surface; c) spin coated onto cuticle surface; d) 10 mM aqueous solution, pH 2.5, 100 µm sample spacing; e) 10 mM aqueous solution, pH 7, 100 µm sample spacing. Note the displayed residual plots have not been chirp corrected.

3. Computational Details and Discussion

3.1. Optimised structures and energy calculations

3.1.1. SDA^{2-}

Figure S3 shows the optimised structures of SDA^{2-} using implicit solvation (i.e. $SDA^{2-}.(H_2O)_0$). The ground state geometry has near C_s symmetry with one of the carboxylate groups out-of-plane (C3-C2-C1-O2 = 99.9°). After excitation to the S_1 state, the main geometry changes are an increase of the C3-C2 bond length and twisting around the allylic bond, enabling a barrierless route to a S_1/S_0 crossing point. This MECP is 1.75 eV lower in energy than the vertically excited S_1 state. At the crossing point, the C4-C3-C2-C1 dihedral angle is 88.6° and both carboxylate groups are rotated out-of-plane.

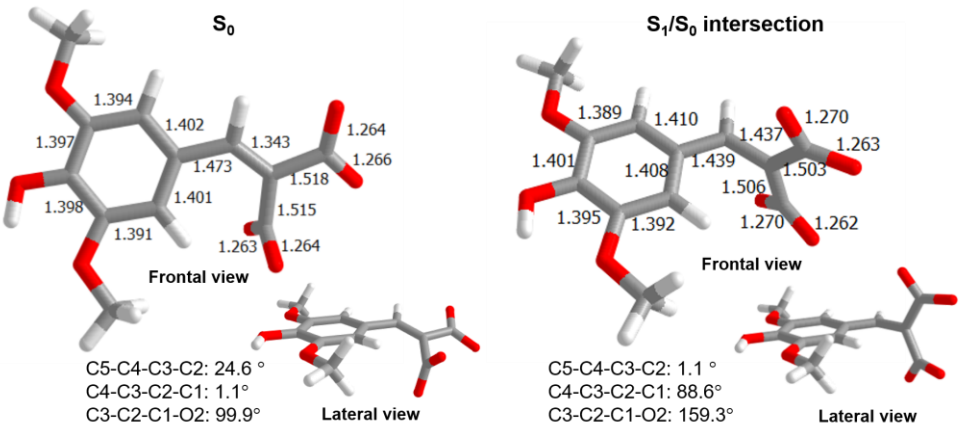

Figure S3. Optimised structures of $SDA^{2-}.(H_2O)_0$ at ωB97XD/6-31+G(d,p), SMD/water.

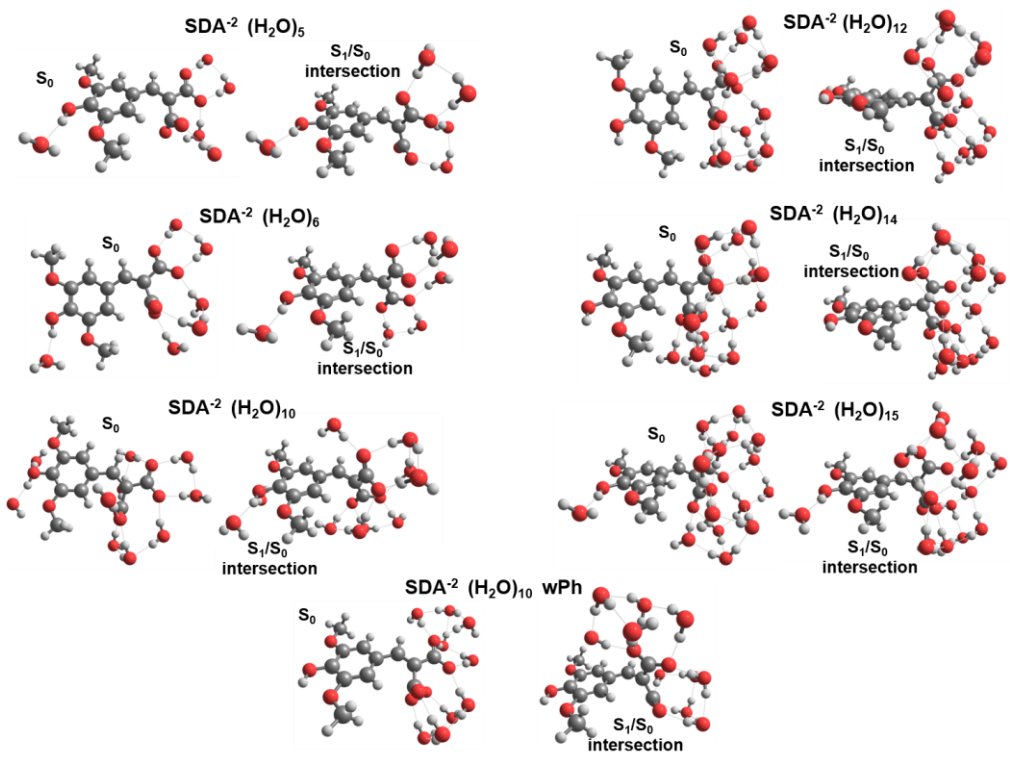

Figure S4. Optimised structures for micro-solvated $SDA^{2-}.(H_2O)_n$ species with n = 5, 6, 10, 12, 14 and 15 calculated at ωB97XD/6-31+G(d,p), SMD/water. wPh denotes all water molecules placed away from the phenyl ring.

Figure S4 shows optimized structures for various micro-solvated $SDA^{2-}.(H2O)_n$ clusters, where n refers to the number of water molecules added (between 5 and 15). No significant structural changes were observed in either the S_0 or S_1 states when compared with $SDA^{2-}.(H2O)_0$. One of the carboxylate groups is out-of-plane in the S_0 state of the clusters, while the optimization of the S_1 state leads directly to a ~90° twisting of the allylic bond. Here, the point where the SCF convergence failed due to the S_1/S_0 energy gap being smaller than 0.1 eV was taken as the S_1/S_0 intersection.

The variation of the absorption and S_1/S_0 MECP energies of $SDA^{2-}.(H_2O)_n$ with changes in the number of explicit water molecules is shown in Figure S5. The systematic inclusion of water molecules seems to have only a minor effect on the excitation energies. In all cases, the S_1 state is the bright ππ* state, while the nπ* state consistently lies at ~5 eV and well above the S_2 state. The addition of explicit solvent results in a modest stabilization of the S_1 and S_2 (ππ*) states and destabilizes the S_3 (nπ*) state, but these changes have no significant impact on the photophysics of the molecule. For $SDA^{2-}.(H_2O)_0$, the calculated S_1–S_0 vertical excitation energy is 4.42 eV (and the oscillator strength f = 0.6623) while for $SDA^{2-}.(H_2O)_6$ the corresponding values are 4.27 eV (and f = 0.73), i.e. slightly higher than the experimental absorption maximum at pH 5.6 (4.06 eV). The adiabatic S_1/S_0 intersection energy (i.e. the energy difference between the ground state optimized minimum and the S_1/S_0 crossing point) mildly changes by the inclusion of explicit solvent (Figure S5, right).

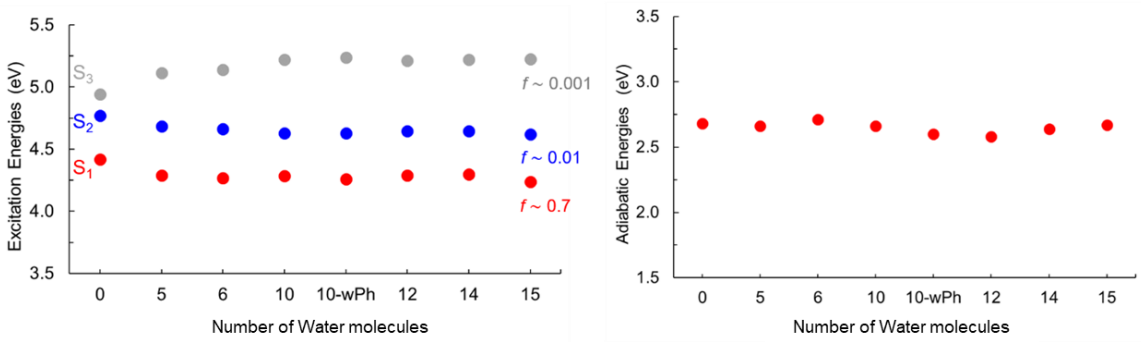

Figure S5. Excitation energies (left) and adiabatic energies (right) of the S_1/S_0 MECP (right) for $SDA^{2-}.(H_2O)_n$ with n = 0 and for various values in the range $5 \leq n \leq 15$ calculated at ωB97XD/6-31+G(d,p), SMD/water. 10-wPh denotes water molecules placed away from the phenyl ring, as shown in Figure S4.

3.1.2. Neutral SDA

The optimised structures of two lowest energy conformers of neutral SDA are shown in Figure S6. The calculated vertical excitation energies from the S_0 state to the S_1, S_2 and S_3 excited states and other key energies are listed in Table S1. SDA_A is the most stable conformer of the ground state molecule; SDA_B, the conformer obtained by twisting the allylic bond by 180°, is ~2 kcal/mol less stable. Both conformers have an intramolecular hydrogen bond which keeps the carboxylic acid groups in the same plane, in contrast with SDA^{2-}, where one of the carboxylates is out of the molecular plane. The main structural difference between the two conformers is that while SDA_A is planar, SDA_B has the two carboxylic acid groups out-of-plane, with a C5-C4-C3-C2 dihedral angle of 31°, resulting from the steric repulsion between the –OH and the closest hydrogen of the phenyl group. This out-of-plane distortion is predicted to cause a modest shift in the S_1–S_0 vertical excitation energy of SDA_B (i.e. a red-shift of the peak absorption wavelength by ~5 nm) and a more dramatic decrease in the associated oscillator strength (0.418 in SBA_B; 0.634 in SBA_A; see Table S1).

Optimising both the SDA_A and SDA_B conformers in the S_1 state brings the molecules to ~90° twisted minimum energy structures ($S_{1\text{-TICT}}$). In both cases, the S_1 to S_0 energy gap at this geometry is only ~0.2 eV (Table S1). Further optimisations of the S_1/S_0 intersection using a penalty function located an S_1/S_0 state crossing only 0.03 eV above the $S_{1\text{-TICT}}$ minimum, with a geometry very similar to this minimum. Photoexcitation preferentially samples the most stable conformer, SDA_A, but the present calculations suggest that subsequent conversion to SDA_B should be an essentially barrierless process, following full 180° rotation around the allylic bond enabled towards, and then after, passing through the S_1/S_0 intersection.

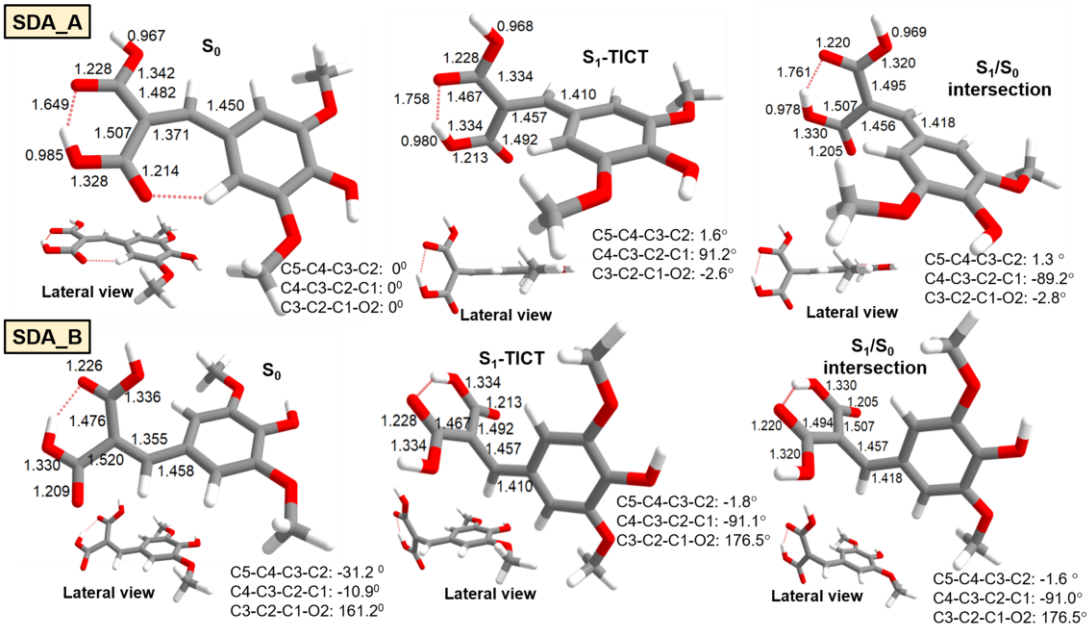

Figure S6. Optimised structures for the S_0 and S_1 states and the S_1/S_0 intersections of the two lowest energy conformers of neutral SDA at ωB97XD/6-31+G(d,p) in the gas phase.

Table S1. Vertical absorption energies and oscillator strengths (*f*) from the S_0 state of the SDA_A and SDA_B conformers to the respective S_n (n = 1-3) states (ΔE_{vert}). The later columns show the energy separation (ΔE) between the S_1 and S_0 states at the S_1 minimum energy geometry ($S_{1\text{-TICT}}$) and the adiabatic energies (ΔE_{ad}) of the $S_{1\text{-TICT}}$ minimum and the S_1/S_0 intersection relative to the S_0 ground state, calculated with ωB97XD/6-31+G(d,p), in the gas phase.

		Vertical excitation energy $S_0 \rightarrow S_n$		Energy separation at $S_{1\text{-TICT}}$ $S_1 \rightarrow S_0$		Adiabatic energy difference	
	State	**State character**	**ΔE_{vert} / eV (*f.osc*)**	**State character**	**ΔE / eV (*f.osc*)**	**State**	**ΔE_{ad} / eV**
SDA_A	S_1	ππ*	3.76 (0.634)	ππ* $_{TICT}$	0.19 (0.000)	S_1 ππ* $_{TICT}$	2.16
	S_2	ππ*	3.96 (0.078)			S_1/S_0-$_{MECP}$	2.18
	S_3	nπ*	4.49 (0.000)				
SDA_B	S_1	ππ*	3.70 (0.418)	ππ* $_{TICT}$	0.19 (0.000)	S_1 ππ* $_{TICT}$	2.05
	S_2	ππ*	4.13 (0.051)			S_1/S_0-$_{MECP}$	2.08
	S_3	nπ*	4.60 (0.004)				

3.1.3. Neutral SDA on the model surface

Four models were built for the interaction of neutral SDA with the 1,21-henicosanediol crystal, a dialcohol.[5] The most stable S_0 optimised geometries are shown in Figure S7 and their relative energies are listed in Table S2. These structures are labelled SDA_{A1} and SDA_{A2} and SDA_{B1} and SDA_{B2}, where the A and B subscripts define the molecular conformation (as in Figure S6) and the 1 and 2 subscripts represent the orientation of SDA relative to the model surface.

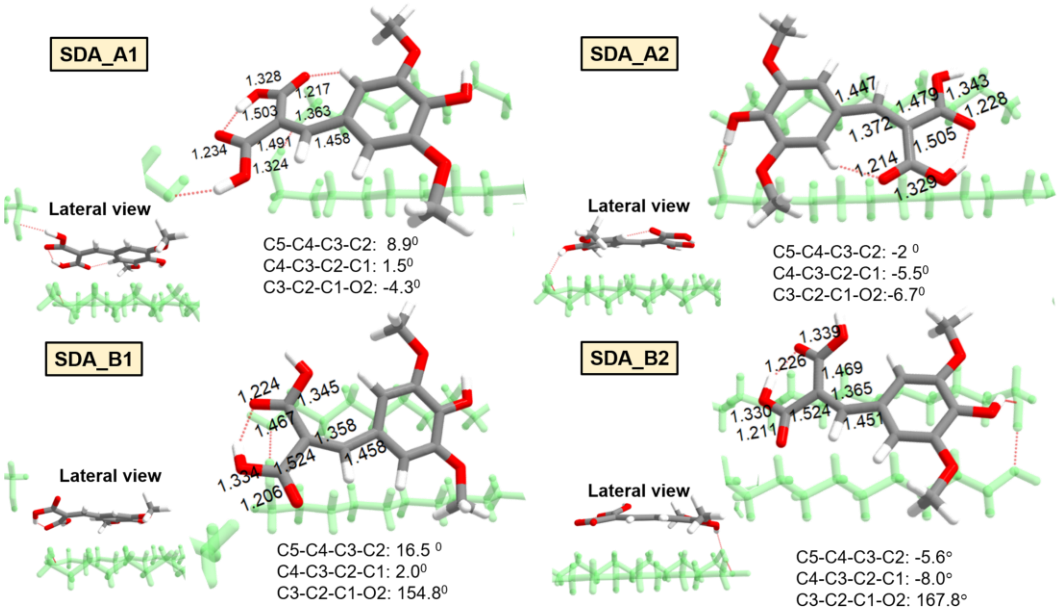

Figure S7. Optimised structures of SDA on the model surface in the ground state, calculated at the DFT/ωB97X-D/6-31G(d) level. The subscripts 1 and 2 define two different arrangements of SDA_A and SDA_B on the model surface. For simplicity, the full structure of the dialcohols that make up the surface is not shown.

Table S2. Ground state absolute energies (in a.u.) and relative energies (in kcal/mol, defined relative to the most stable conformation, i.e. SDA_A in the gas phase and SDA_{A1} on the surface), and respective excitation wavelengths and oscillator strengths for transitions to the two lowest energy excited states.

	S_0 Abs (a.u.)	S_0 Rel (kcal/mol)	S_1 / nm	*f.osc*	S_2 / nm	*f.osc*
SDA_A	-990.8010	0	330	0.63	313	0.08
SDA_{A1}	-3919.6626	0	320	0.64	299	0.05
SDA_{A2}	-3919.6531	5.96	342	0.68	323	0.01
SDA_B	-990.7973	2.32	335	0.42	301	0.05
SDA_{B1}	-3919.6358	16.82	322	0.59	293	0.04
SDA_{B2}	-3919.6495	8.22	342	0.61	313	0.02

Ground state geometry optimisation shows that: i) conformers A are more stable than conformers B on the top of the model surface (as observed in the gas phase); ii) for conformer A, the most stable orientation on the model surface (by 0.26 eV), has the –COOH group interacting with an OH of the dialcohol (SDA_{A1}); and iii) for conformer B, the most stable orientation has the phenolic hydrogen bonded to the model surface with the –COOH groups free with respect to the model surface.

Table S2 (and Figure S8) also shows the excitation energies for the different conformers. SDA_{A1} and SDA_{B1} are predicted to have similar $S_0 \rightarrow S_1$ excitation energies; the corresponding wavelengths are in excellent agreement with absorption maxima measured for the thin film samples and for SDA in aqueous solution at low pH (325 nm). The predicted $S_0 \rightarrow S_1$ absorption maxima are slightly blue-shifted relative to those calculated for bare SDA in the gas phase (SDA_A and SDA_B), whereas those for the less stable conformers (SDA_{A2} and SDA_{B2}) are mildly red-shifted. Overall, however, introducing the model surface has no great impact on the excitation energies – again consistent with the experimental observations.

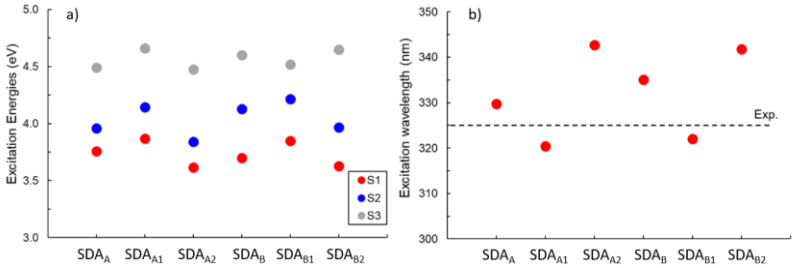

Figure S8. Excitation energies (in eV and nm) computed for the neutral SDA in the gas phase (SDA_A and SDA_B) and on the wax surface (SDA_{A1}, SDA_{A2}, SDA_{B1}, and SDA_{B2})

3.2. Reaction coordinates

3.2.1. SDA^{2-}

The topographies of the potential energy curves (PECs) for SDA^{2-} were characterised by linear interpolations in internal coordinates (LIICs) connecting the vertically excited S_1 (ground state geometry) and the S_1/S_0 intersections, as shown for the dianion in Figure S9. The PECs with and without explicit solvation are similar.

In both cases, after excitation to the bright S_1 state, the molecule undergoes a barrierless relaxation towards an S_1/S_0 intersection, which is ~2.7 eV above the S_0 minimum. As discussed earlier, the dominant geometry change that brings the molecules to this intersection is twisting around the allylic bond. As the molecule twists, the S_1 to S_0 oscillator strength decreases, reaching a value close to zero around the intersection. Note that, although the PECs with and without explicit solvent are energetically similar, the presence of strongly interacting water molecules (via hydrogen bonding with SDA^{2-}) effectively doubles the mass-weighted coordinate. Thus, solvent interaction can be expected to slow the evolution to the S_1/S_0 intersection (*cf.* for the isolated dianion).

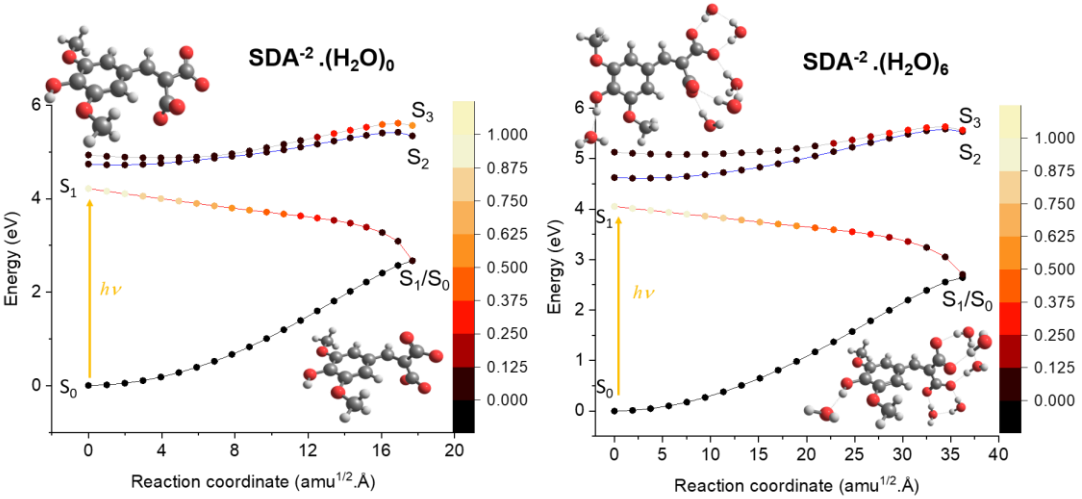

Figure S9. Potential energy curves for $SDA^{2-}.(H2O)_0$ and $SDA^{2-}.(H2O)_6$, calculated at TD-ωB97XD/6-31+G(d,p) using SMD/water along a LIIC starting from the vertically excited S_1 state to the S_1/S_0 MECP. The points along the excited-state reaction pathway are coloured according to their relative oscillator strength (*f*), shown by the false colour scale to the far right of each panel.

3.2.2. Neutral SDA

PECs for neutral gas phase SDA calculated along a LIIC linking the vertical excitation region of the S_1 state and the S_1/S_0 intersection show a barrierless relaxation path out to the S_1-TICT geometry, accompanied by a large energy stabilisation (Figure S10). The S_1 PECs for the SDA_A and SDA_B conformers both start with a rather flat region upon leaving the Franck-Condon region, but no minimum (i.e. a stationary point with no negative frequencies) was found around this region. An S_1/S_0 intersection was found only 0.03 eV above this minimum, with minimal changes in the geometry with respect to S_1-TICT. After reaching this intersection, twisting around the allylic bond can give rise to both the SDA_A and SDA_B conformers. As noted earlier, the biggest difference between these conformers is the relative positions of the –COOH groups relative to the phenol plane: in SDA_B the planarity is broken by steric repulsion and, in this case, the mass-weighted distance from the vertically excited geometry to the S_1/S_0 intersection is smaller.

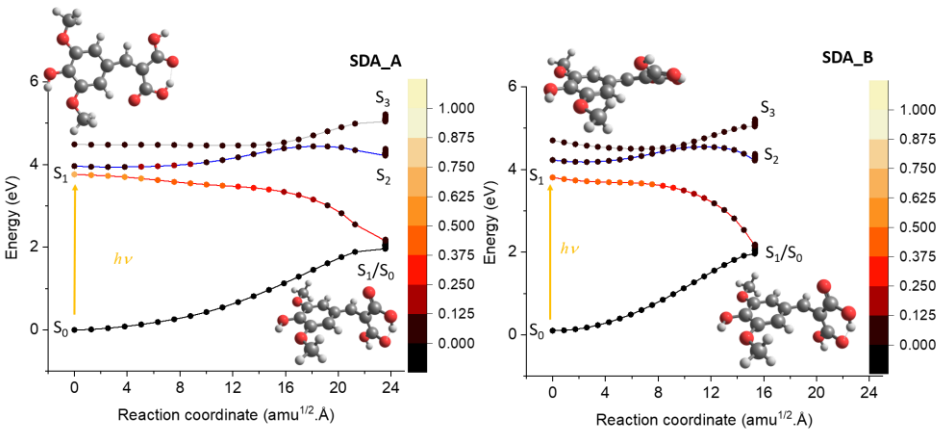

Figure S10. PECs for gas phase SDA_A and SDA_B along a LIIC linking the vertically excited S_1 state to the S_1/S_0 intersection, calculated at the TD-ωB97XD/6-31+G(d,p) level. The points along the excited-state reaction pathways are coloured according to their oscillator strengths (*f*) from the S_0 state transitions. The oscillator strength values are coloured according to the scale showed in the insert.

3.3. Charge transfer character in the excited states of SDA^{2-} and SDA

The charge-transfer (CT) character of the lowest singlet excited states of SDA^{2-} and SDA were evaluated by computing the charge-transfer descriptor, the q(CT) number, at the ωB97XD/6-31+G(d,p) level, using the TheoDORE program.[6] For SDA^{2-}, implicit solvation was used (SMD/water), while gas phase calculations were used for neutral SDA. q(CT) numbers range from 0 to 1 and are calculated over user-defined molecular fragments; q(CT) values closer to 1 imply a state with greater CT character, values closer to zero imply smaller CT character. Calculated q(CT) numbers for SDA^{2-} (bare, and when complexed with six H_2O molecules), for the bare SDA_A and SDA_B conformers, and for both conformers atop the model surface are shown in Table S3. The natural transition orbitals (NTOs) that characterise these transitions are shown in Figure S11.[6] In all cases, the S_1 state formed by vertical excitation has a q(CT) number of ~0.4, i.e. is a locally excited state. But, after geometric relaxation on the S_1 state, this state acquires strong charge transfer character (q(CT) ~0.8). As no S_1 minimum was found for SDA^{2-}, the reported q(CT) number was computed at geometries close to the S_1/S_0 intersection.

Table S3. *q*(CT) number for the S_n (***n*** = 1-3) excited states obtained at the TD-DFT/ωB97XD/6-31+G(d,p) level of theory, at the ground state equilibrium geometry (Geom S_0) and after relaxation to the S_1 minimum energy geometry (Geom S_1). The inserted figures show the molecular fragments used to compute *q* (CT).

	$SDA^{2-}.(H_2O)_0$		$SDA^{2-}.(H_2O)_6$		SDA_A	SDA_A	SDA_{A1}	SDA_{A2}	SDA_B	SDA_B	SDA_{B1}	SDA_{B2}
	Geom S_0	Geom S_1	Geom S_0	Geom S_1	Geom S_0	Geom S_1	Geom S_0	Geom S_0	Geom S_0	Geom S_0	Geom S_0	Geom S_0
S_1	0.41	0.80	0.40	0.79	0.37	0.82	0.37	0.39	0.40	0.82	0.39	0.38

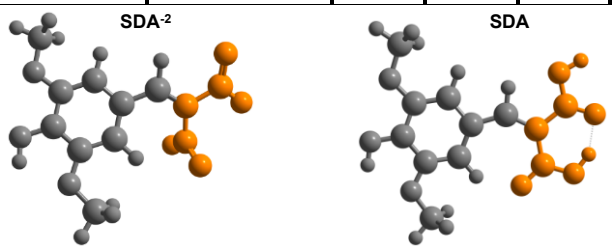

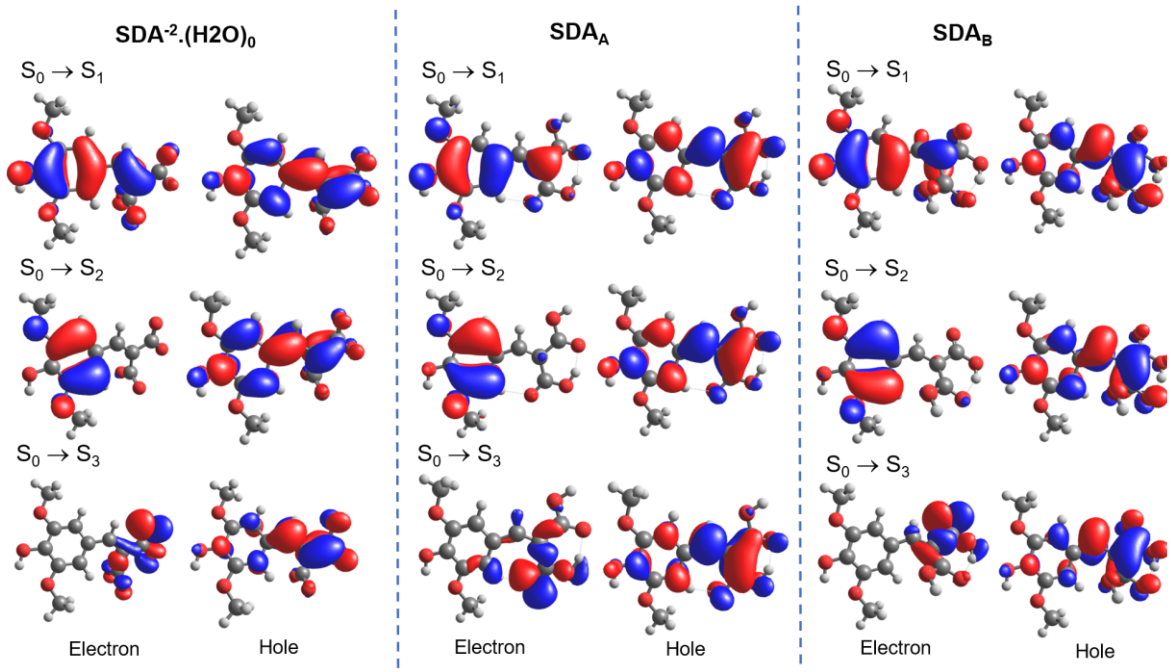

Figure S11. Natural transition orbitals for the three lowest vertical excitations of SDA^{2-}, SDA_A and SDA_B calculated at ωB97XD/6-31+G(d,p), using SMD/water for the dianion and gas phase calculations for neutral SDA.

4. Additional Transient Absorption Data

Transient absorption (TA) data shown in Figure S12 for: a) SDA in bulk solution against the substitute cuticle wax surface excited at 305 nm (lifetimes derived from which are included in Table 1 of the main paper); b) pH 2.5, exciting at 320 nm; and c) pH 7, exciting at 305 nm. a)-c) display similar features and lifetimes. To note, at pH 2.5, the SDA is present in its neutral form.

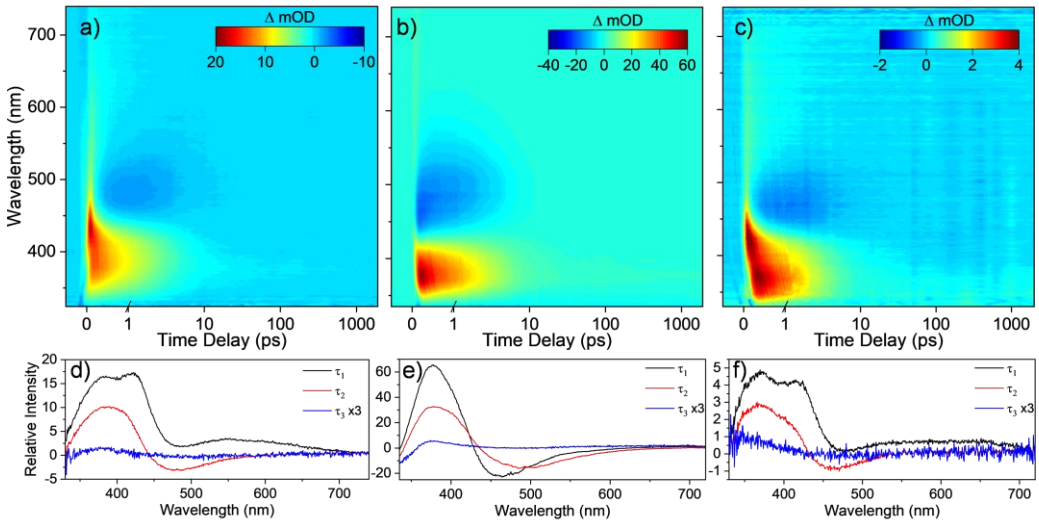

Figure S12. TAS data displayed as false colour heat maps of a) SDA^{2-} at pH 5.6 at 10 mM concentration with a sample path length of 6 µm against the substitute wax cuticle surface, photoexcited at 305 nm; b) SDA at pH 2.5 at 10 mM concentration with a path length of 100 µm, photoexcited at 320 nm. c) SDA^{2-} at pH 7 at 10 mM concentration with a path length of 100 µm, photoexcited at 305 nm. Panels d) to f) show the evolutionary associated difference spectra (EADS) extracted from the global sequential fits to the data shown in a), b) and c), respectively.

Table S4. Extracted lifetimes from the global sequential fit of the ultrafast spectroscopy data with errors reported to twice the standard error.

Sample	τ_1 (fs)	τ_2 (ps)	τ_3 (ns)
pH 2.5 (SDA)	460 ± 40	3.33 ± 0.04	>> 2
pH 7 (SDA^{2-})	420 ± 40	2.51 ± 0.04	>> 2

Evidence for ground state vibrational cooling of SDA^{2-} in aqueous solution is shown in Figure S13. The arrow highlights the shifting nature of the excited state absorption (ESA) in the transient absorption spectra (TAS) following the initial relaxation out of the Franck-Condon region and through the conical intersection (CI).

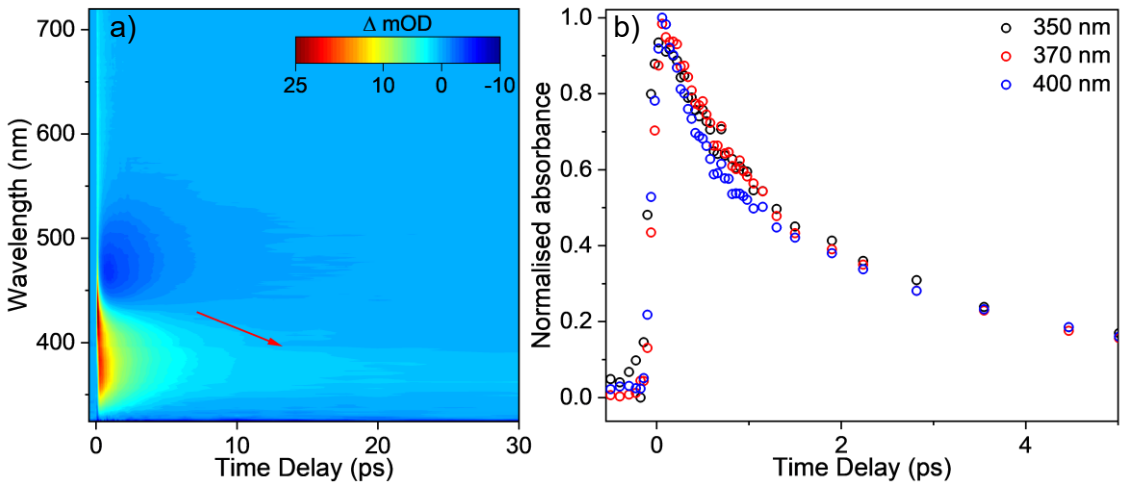

Figure S13. a) Early time TAS data displayed as a false colour heat map for a bulk aqueous solution of SDA^{2-} at pH 5.6 at 10 mM concentration with a sample path length of 100 µm, photoexcited at 305 nm. The red arrow highlights the time-dependent ESA spectrum, which is not captured by the fitting procedure following repopulation of the S_0 state within the τ_2 time constant. b) Time profiles of selected wavelengths showing the shorter lifetime of longer wavelengths, indicative of vibrational cooling.

References

1 L. Walmsley, L. Waxer and C. Dorrer, *Review of Scientific Instruments*, 2001, **72**, 1–29.

2 M. P. Grubb, A. J. Orr-Ewing and M. N. R. Ashfold, *Review of Scientific Instruments*, 2014, **85**, 064104.

3 J. J. Snellenburg, S. P. Laptenok, R. Seger, K. M. Mullen and I. H. M. van Stokkum, *J Stat Softw*, 2012, **49**, 1–22.

4 K. M. Mullen and I. H. M. van Stokkum, *J Stat Softw*, 2007, **18**, 1–46.

5 N. Nakamura, K. Uno and Y. Ogawa, *Acta Crystallographica Section C*, 2000, **56**, 1389–1390.

6 F. Plasser and H. Lischka, *J Chem Theory Comput*, 2012, **8**, 2777–2789.